Catalysis Today 423 (2023) 114266

Contents lists available at ScienceDirect

Catalysis Today

journal homepage: www.elsevier.com/locate/cattod

Ruthenium deposited onto graphitic carbon modified with boron for the intensified photocatalytic production of benzaldehyde

Rafael R. Solís, M. Alejandra Quintana, Gabriel Blázquez *, Mónica Calero, Mario J. Muñoz-Batista *

Department of Chemical Engineering, University of Granada, 18074 Granada, Spain

ARTICLE INFO

Keywords:
Graphitic carbon nitride
Boron
Ruthenium
Benzaldehyde
Photocatalysis

ABSTRACT

The selective oxidation of added-value aromatic alcohols into aldehydes of high interest via photocatalysis has been postulated as a green and competitive oxidative reaction at mild conditions. This work is focused on the design of a tertiary graphitic carbon nitride (g-C_3N_4) based photocatalysts competitive for the photocatalytic production of benzaldehyde in an aqueous solution. The polymeric g-C_3N_4 has been modified in an easy one-pot green synthesis scheme, with the incorporation of boron in the polymeric structure and the deposition of ruthenium nanoparticles. The Ru ratio within 0.5–4% was assessed. The photocatalysts were fully characterized (XRD, FTIR, XPS, N_2 isotherms, DRS-UV–visible, and PL) and the photocatalytic activity was assessed in the oxidation of benzyl alcohol to benzaldehyde in an aqueous solution. The incorporation of boron enhanced the selectivity towards benzaldehyde due to enhanced separation charges suggested by the photoluminescence technique; whereas ruthenium improved the reaction rate of the alcohol, affecting negatively the selectivity though. The sample containing 1% of Ru was selected as the optimum in terms of selectivity. The relative contribution of the involved reactive oxidant species was assessed by chemical scavenger tests, highlighting the contribution of the photo-generated holes followed by $O_2^{\bullet-}$. The analysis of the band's alignment of the g-C_3N_4 before the modification with boron and ruthenium supports the enhancement by rising the redox potential of the holes released in the valence band.

1. Introduction

Aromatic aldehydes are organic substances bearing an aromatic ring and a formyl substituent. These organic substances are of paramount interest since are used in the industry of dyes, fragrances, and flavoring in the food industry or as pharmaceutical precursors. Benzaldehyde (C_6H_5CHO) has paramount relevance in organic synthesis as a raw material, for instance, it is widely used to flavor almonds, as an additive in personal care products, and in dye manufacturing, as an additive due to its antibacterial or antifungal properties. At large scale, benzaldehyde is synthesized from the hydrolysis of benzal chloride or the air oxidation of toluene. The current industrial process of benzaldehyde manufacturing involves the oxidation of toluene, either in the vapor or liquid phases. Nonetheless, the procedure requires rather high temperatures and pressures, leading to low yields due to the formation of by-products [1]. Milder conditions can be obtained if catalysts are used in the oxidation process [2].

Photocatalysis emerges as an environmentally friendly alternative for the production of aldehydes of high interest under a greener approach, at mild temperature and pressure conditions, without requiring additional solvents as other technological alternatives [3]. Furthermore, the use of semiconductors active under radiation sources of low-energy such and renewable as sunlight or UVA potentiates the interest in this alternative. Titanium dioxide has been largely researched in the photocatalysis field due to its potential semiconductor properties; however, photoexcitation is limited to the UV region and inefficient separation of photogenerated charges [4]. As a consequence of the effort paid in the development of new potential semiconductors, graphitic carbon nitride (g-C_3N_4) appeared as a promising alternative with a lower bandgap (2.7 eV) if compared to the benchmark titania polymorphs due to the improved absorption in the visible region and tunable structure to improve the electronic and optical properties [5,6]. The graphitic g-C_3N_4 is built by aromatic nitrogen-containing heteroatoms scaffolded with tris-s-triazine units which are interconnected via tertiary amines,

* Corresponding authors.
E-mail addresses: gblazque@ugr.es (G. Blázquez), mariomunoz@ugr.es (M.J. Muñoz-Batista).

https://doi.org/10.1016/j.cattod.2023.114266
Received 30 March 2023; Received in revised form 30 May 2023; Accepted 12 June 2023
Available online 15 June 2023

with a unique delocalized stacking of C_3N_4 layers and high electronic conductivity. Among the diverse applications in the field of photocatalysis, g-C_3N_4 has been studied as a candidate for the photocatalytic production of benzaldehyde [7–9] . The energy of valence and conduction bands compromises an alignment that promotes the reduction of O_2 into superoxide radical but is unable to generate hydroxyl radical, which launches the unselective oxidation of alcohols [10]. The tunable structure of g-C_3N_4 has been proven effective to develop imperfections which leads to the enhance the harvesting of radiation and improves the separation of photogenerated charges via non-metal doping [11,12]. Among them, the modification with boron has been demonstrated to raise the selectivity of benzaldehyde formation from benzyl alcohol oxidation [13]. Furthermore, the deposition of low amounts of noble metals such as Au, Pd, Pt, Ag, Ir, Rh, or Ru onto the g-C_3N_4 supports the improvement of the reaction rate, upgrading the separation charges [14–18]. The presence of metal nanoparticles can act as electron sinks to capture photoinduced electrons from the conduction band of g-C_3N_4 [19].

This work develops the preparation of a ternary-modified g-C_3N_4 photocatalyst in a one-pot-step synthesis scheme applied for the photocatalytic oxidation of benzyl alcohol to benzaldehyde. Two modifications have been included in the structure of g-C_3N_4 simultaneously; firstly, with boron modification aimed at the enhancement of benzaldehyde selectivity; and secondly, Ru deposition for the raise of the conversion of benzyl alcohol. Different boron-modified g-C_3N_4 samples under Ru loading within 0.5–4% (at. wt) were prepared and characterized with XRD, FTIR, N_2 isotherms, DRS-UV–visible and photoluminescence techniques. The activity towards benzyl alcohol oxidation was tested, assessing the alcohol conversion and selectivity to the aldehyde production to optimize the metal loading. The oxidation mechanism in terms of the reactive oxidant species involved in the process was accomplished for the optimized Ru content in terms of benzaldehyde selectivity.

2. Experimental section

2.1. Materials and catalyst synthesis

The chemicals used were analytical grade at least, acquired from Merck®, and used as received. HPLC-quality acetonitrile was used as a mobile phase in chromatographic analysis. Ultrapure water (18.2 MΩ·cm) from a Direct-Q®-UV device (Millipore®) was used for the preparation of all the solutions.

The graphitic carbon nitride (g-C_3N_4, CN) was synthesized from pyrolysis of melamine (rate 10 ºC·min^{-1}, holding temperature 500 ºC, 2 h). As a result, a yellowish solid was obtained. This solid was suspended in water to discharge those particles that are not successfully suspended in the solution. The suspended particles were collected by filtration and dried at 80 ºC. The boron-modified CN was prepared by pyrolysis under an N_2 atmosphere as described in a previous study. CN and $NaBH_4$ were mixed at the same mass ratio and grounded in a mortar. The mixed powder was next calcined at 450 °C (ramp 10 °C min^{-1}, 1 h). The resulting brownish material (NaBCN) was cooled down to room temperature, washed several times with water, and dried at 80 °C. The NaBCN samples with ruthenium deposited were prepared following a similar procedure in which $NaBH_4$ played a double role, as both boron precursor and reduction agent. Thus, CN and $NaBH_4$ were mixed at equal mass ratios in a mortar. Next, a desired amount of ruthenium was added as $RuCl_3$, and dissolved in 0.9 mL of water. This volume was estimated to carry out an incipient wetness impregnation method over 1.5 g of solid NaBCN. The ruthenium solution was dropwise added to the mixed powder wetting all the solid particles. Next, the wet solid was calcined at 450 ºC (heating rate, 10 °C min^{-1}, 1 h). The resulting solid was cooled down, washed, and dried as done with the NaBCN blank sample. The samples containing ruthenium were labeled as NaBCN-xRu where x stands for the atomic ruthenium to mass percentage in the sample.

2.2. Characterization of the catalysts

The crystalline structure was analyzed using powder X-Ray Diffraction (XRD) in a Bruker D8 Discover device working with a Cu Kα radiation source (λ = 1.5406 Å), equipped with a detector Pilatus3R 100 K-A registering within a 2θ range of 6–80° at a rate of 0.04° min^{-1}. The software QualX® and the Crystal Open Database (COD) were used for the identification of the crystal phases in the obtained diffractograms.

The structure was further studied by the stretching of the bonds by Fourier Transform InfraRed (FTIR) analysis, displayed in a Perkin-Elmer model Spectrum65 device within 400–4000 cm^{-1}.

The surface porous properties were assessed by N_2 adsorption–desorption at 77 K performed in a Sync 200 equipment from 3 P Instruments©. Samples were degassed overnight at 150 ºC under a vacuum. The specific surface area was obtained by the Brunauer-Emmett-Teller method (S_{BET}), and the total specific pore volume (V_T) was calculated from the N_2 uptake at p/p_0~0.99. The Barrett, Joyner, and Halenda method (BJH) was applied to analyze the average (4 V/A) and most frequent (dV/dD) pore diameter.

X-ray Photoelectron Spectroscopy (XPS) was applied for the study of the elemental composition present at the surface of the materials in a Kratos AXIS UltraDLD device working with an X-ray source from Al Kα. The spectra were referenced to the C1s peak of adventitious carbon to 284.6 eV. The software XPSpeak 4.1® was used for the deconvolution of the peaks, considering a Shirley background correction.

The optical properties were assessed through Diffuse Reflectance Spectroscopy (DRS) in the UV–visible region in a Varian Cary 5E spectrophotometer. The Kubelka-Munk Function, $F(R_\infty)$, was obtained from the reflectance spectra, and the bandgap was estimated from the Tauc plot method considering indirect electron transitions [20]. The recombination rate of the photo-generated electrons was assessed by photoluminescence (PL) analysis in a Varian Cary Eclipse device under an excitation wavelength of 365 nm.

2.3. Photocatalytic experiments

The NaBCN-Ru catalysts were tested for the selective photocatalytic oxidation of benzyl alcohol to benzaldehyde in a borosilicate glass annular jacketed photoreactor equipped with two UVA lamps emitting at 365 nm (9 W each). Detailed information on the experimental setup can be found in a previous work [21]. The lamps were centered in the inner space and the aqueous solution with the slurry catalyst was circulating by the jacketing space. The slurry was constantly pumped from an auxiliary jacketed tank, cooled with water to 20 ºC, in which the catalyst was kept suspended through magnetic stirring in the bottom. To ensure O_2 saturation, the air was bubbled in the auxiliary tank. The radiation reaching the liquid phase was quantified by an in situ chemical actinometry, based on the photo-reduction of ferrioxalate complex combined with a polyoxometalate salt ($Na_2SiW_{12}O_6$) to monitor the temporal abatement of the ferrioxalate complex into CO_2 [22]. The actinometry tests were carried out with oxalic acid 60 mM, $FeCl_3{\cdot}6\ H_2O$ 5 mM, and $H_4SiW_{12}O_{40}$ 1 mM. The pH of the solution was adjusted to 4.5 with the addition of diluted 0.1 M HCl and NaOH to avoid the plausible auto-decomposition of the polyoxometalate complex. Taking into account the quantum yield value during the photo-production of $(SiW_{12}O_{40})^{5-}$ ($\phi = 0.18$ mol·Einstein^{-1} at 365 ± 10 nm) [22], the radiation intensity value estimated was $I_0 = (3.5 \pm 0.2) \times 10^{-4}$ Einstein $L^{-1}{\cdot}min^{-1}$.

The photocatalytic tests of benzaldehyde production started by loading the aqueous solution of benzyl alcohol 0.5 mM. After, the photocatalyst was added at a dose of 0.5 g·L^{-1} in the auxiliary tank until homogeneously dispersed the solid in the reaction system. Before the irradiation, an adsorption step of 30 min was displayed in the darkness. Next, the lamps were switched on, and samples were regularly extracted

for analysis. The photocatalyst was removed from the extracted samples by syringe filters (PVDF, 0.45 μm).

The concentration of the aromatic alcohols and their aldehydes was quantified by High-Pressure Liquid Chromatography (HPLC) in an HPLC Alliance e2695 from Waters™ coupled to a 2998 photodiode array UV–visible detector. The stationary phase consisted of a Zorbax Bonus-RP column (4.6 ×150 mm, 5 μm). The mobile phase, pumped at 1 mL min^{-1}, was fed under an isocratic program with 90 μL of sample injection. For the analysis of benzyl alcohol (BA) and benzaldehyde (BD), a mixture of 30% acetonitrile (A) and 70% acidified water (B, 0.1% v/v trifluoroacetic acid) was pumped, conducting the quantification at 215 for BA and 248 for BD.

The temporal evolution of BA abatement was adjusted to a pseudo-first order kinetics, and the observed constant (k_{BA}) was calculated as a mere tool of comparison between the performances of the NaBCN-Ru samples. Also, the selectivity (S) as calculated from the BD profiles, and an average value during the whole period tested was calculated as follows:

$$S_{average} = \frac{\int S(t)dt}{(t-0)} \quad (1)$$

The quantum efficiency (Q_E) of BA photo-degradation was quantified, following the IUPAC recommendations [23–25], which defines the Q_E as the ratio of the number of molecules reacting through the reaction rate ($r_{BA,0}$), by the number of the photon which interacts with the catalyst, i.e. the photon absorption rate ($e^{\alpha,\nu}$) [26]:

$$Q_E = \frac{r_{BA} \quad (mol \quad m^{-3} \quad s^{-1})}{e^{\alpha,\upsilon} \quad (Einstein \quad m^{-3} \quad s^{-1})} \quad (2)$$

where $r_{BA,0}$ was estimated from the slope of the temporal evolution of the C_{BA} with the tangent at the initial reaction time. The determination of the photon absorption rate ($e^{\alpha,\nu}$), and the radiative transfer equation (RTE) was solved considering the geometry of the used photoreactor [21]. Firstly, the determination of the optical properties of the catalytic suspensions is required. Detailed description of the mathematical procedure for both optical properties and photon rate estimations are provided in previous works [13,21].

The contribution to the BA oxidation by the reactive species generated during the photocatalytic process was assessed by adding different chemical scavengers. The influence of superoxide radical was investigated with N_2 bubbling, or the addition of p-benzoquinone (pBQ, 1 mM) or disodium 4,5-dihydroxybenzene-1,3-disulfonate (tiron, 1 mM). The contribution of hydroxyl radicals was assessed by adding tert-butyl alcohol (TBA, 10 mM) while photo-generated holes were suppressed under the presence of oxalic acid (OA, 10 mM). These assays were conducted following the same procedure as the blank test and adjusting to the same initial pH value (pH=9 ± 0.5).

3. Results and discussion

3.1. Characterization of the NaBCN-Ru photocatalysts

Fig. 1 **A** depicts the changes registered in the crystalline structure of the CN after boron modification and Ru deposition. The XRD pattern of the CN sample displayed the two main characteristic peaks generated as a consequence of the polycondensation of melamine to generate the tris-s-triazine units [27]. The main peak, located at around ~27°, reports the (002) plane defined by the interplanar aromatic layers from π-π * interactions of the heptazine rings. A secondary peak, much less intense, placed at ~13°, is attributed to the (100) plane, whose presence is reported by the intralayer spacing of the heptazine rings. The incorporation of boron in the CN structure led to a considerable decrease in both XRD peaks due to the partial loss of crystallinity in the structure [28], as shown in the pattern for NaBCN. The Ru deposition in the presence of $NaBH_4$ led to NaBCN-Ru samples, which led to the complete removal of the intralayer heptazine (100) facet, suggesting a high distortion of the in-plane aromatic structure [29]. The Ru doping in the CN structure has been reported in the literature at low Ru loadings, which explains the deformation of the crystalline in-plane of the heptazine rings given to the disappearance of the (100) facet in their XRD pattern [16,29]. Moreover, the interplanar (002) peak considerably diminished its intensity, probably due to the partial loading of ruthenium, as already reported in the literature for other Ru modifications of CN materials [30,31]. A Rietveld refinement of the XRD patterns led to detect the presence of halite, NaCl (COD 00–900–8678), in all the samples containing Ru, as a consequence of the reaction between chloride and sodium, respectively contained in Ru and boron precursors,

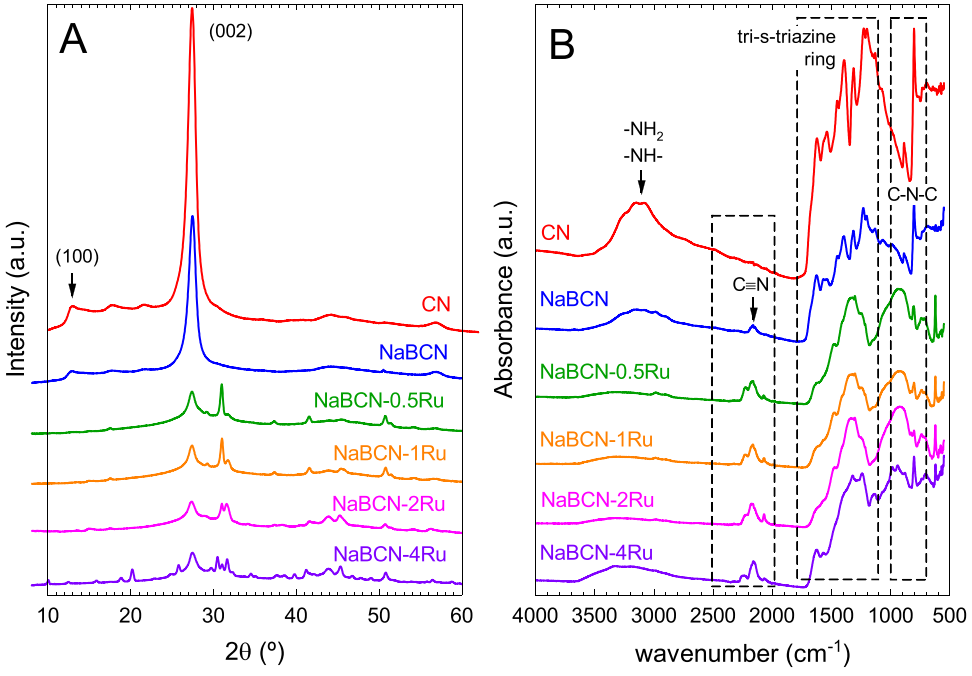

Fig. 1. XRD patterns (A) and FTIR spectra (B) of NaBCN-Ru samples.

$RuCl_3$ and $NaBH_4$. Furthermore, the sample with the highest content of Ru, namely NaBCN-4Ru, also displayed the presence of tricalconite, $Na_6[B_4O_5(OH)_4]_3{\cdot}8\ H_2O$ (COD 00–900–2675). However, no metallic Ru peaks were identified, probably due to the low intensity they may appear [30–32], especially taking into account the possible overlapping problems with NaCl and tricalconite.

The structural modification of the CN structure with both B and Ru incorporation was further analyzed by FTIR, see Fig. 1**B**. The distortion of the intraplanar heptazine rings with Ru insertion can be corroborated in the FTIR footprint of NaBCN-Ru samples. The peals were smoothed, with an important loss of their definition. The CN sample displayed well-defined broadband at 3000–3500 cm^{-1}, attributable to -NH_2 and -NH-groups [33]. Also, the CN spectrum showed a peak at ~ 810 cm^{-1}, reported by the out-of-plane bonding vibration characteristics of the condensed triazine units [34]. The modification with boron of the graphitic structure of the carbon nitride led to a great depletion of this band. A group of peaks within 900 and 1800 cm^{-1} defined by the vibration of the aromatic C-N rings of the heptazine units were fully registered in the CN sample [35]. The intense peaks at 1620, 1530, and 1390 cm^{-1} can be assigned to the aromatic C-N stretching vibration, whereas the peaks at 1310 and 1230 cm^{-1} appear due to the stretching vibration of C-N-(C)-C or C-NH-C bonds, respectively [36,37]. The modification with boron considerably modified the intensity of these peaks, but still, the characteristic footprint registered in the pristine CN was recognized in the NaBCN sample. However, the further addition of Ru particles erased the defined pattern peaks of the heptazine units.

The textural properties of samples were analyzed by N_2 adsorption-desorption isotherms at 77 K. The isotherms are depicted in Fig. 2 and the main characterization results are shown in Table 1. The N_2 physisorption isotherms in the samples described the typical type IV pattern behavior with H3 hysteresis loops [38–40], characteristic of mesoporous with aggregates of plate-like particles [41]. The BET surface area of all the samples was below 10 $m^2\ g^{-1}$, typical reported values for graphitic carbon nitride prepared from the polymerization of melamine [42]. A slight mesoporosity was registered in the hysteresis loops with an average pore size of around 3 nm. The modification of the original CN sample either with B and Ru led to a decrease in the surface properties, i.e. BET area pore volume.

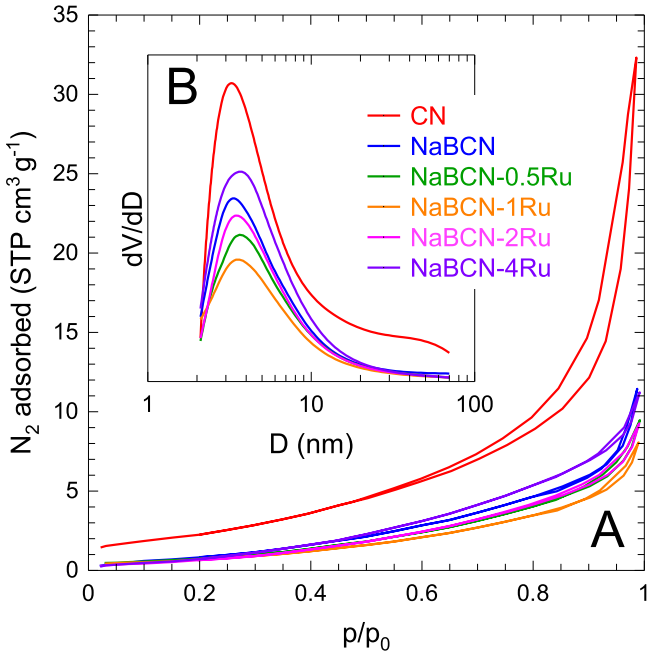

Fig. 2. N_2 adsorption-desorption isotherms (A) and BJH pore size distribution (B) of NaBCN-Ru samples.

Table 1
Textural and optical properties of the NaBCN-Ru samples.

Sample	S_{BET} ($m^2\ g^{-1}$)	V_T ($cm^3\ g^{-1}$)	$D_{average}$ (nm)	$D_{frequent}$ (nm)	E_{BG} (eV)	E_{VB} (eV)
CN	9.1	0.050	30.2	3.5	2.7	1.0
NaBCN	4.0	0.018	13.2	2.9	2.6	1.3
NaBCN-0.5Ru	3.1	0.014	11.9	3.5	2.4	-
NaBCN-1Ru	2.9	0.012	11.9	3.5	2.3	1.9
NaBCN-2Ru	2.8	0.014	10.6	2.9	2.0	-
NaBCN-4Ru	2.5	0.017	9.2	3.9	2.6	-

S_{BET}: total specific surface area by BET method; V_T: total pore volume; $D_{average}$ and $D_{frequent}$: average and most frequent pore diameter by BJH method, respectively; E_{BG}: bandgap by Tauc plot method; E_{VB}: valence band energy by XPS.

The chemical nature of the surface of CN, NaBCN, and NaBCN-4Ru samples was assessed by the XPS technique. The high-resolution XPS spectra of C1s, N1s, B1s, and Ru3p are depicted in Fig. 3. As illustrated, the incorporation of B and Ru highly modifies the XPS spectra due to the structural changes incorporated. The spectra were deconvoluted following the contributions reported in the literature for graphitic carbon materials. The C1s peak of g-C_3N_4 is commonly deconvoluted in sp^2 N = C-N (287.9 eV), sp^3 C-C/C-N (285.2 eV), and sp^2 C-C/C=C (284.4 eV) bonds [43]. The sample CN displayed a major contribution of sp^2 carbon in the form of N = C-N bonds. The bonds attributable to sp^3 C-C/C-N or sp^2 C-C/C=C raised their relative contribution with the modification with boron as shown in NaBCN and NaBCN-4Ru samples. Moreover, a secondary peak regarding $Ru3d_{3/2}$ appeared at an energy of ~280 eV [44]. The Ru3d core levels overlap the C1s region, making difficult the analysis of Ru species by exclusive analysis of Ru3d. For that reason, the Ru3p level, equally accessible as Ru3d, was analyzed for the study of the oxidation state of Ru. The peaks in Ru3p were successfully assignable to Ru $3p_{3/2}$ (484.0 eV) and $3p_{1/2}$ (461.1 eV) of metallic Ru^0 [44–47]. The N bonds were analyzed in the N1s region, considering the following contributions C_3–N ($N_{3\ C}$, 399.9 eV), N–C=N ($N_{2\ C}$, 398.4 eV), N–H_x (401.0 eV) and B=N-C (399.0 eV) [28,43,48,49]. The CN samples presented a high contribution of N contained in the aromatic rings ($N_{2\ C}$), tertiary N ($N_{3\ C}$), and a small proportion of terminal NH_x was observed. The NaBCN samples displayed the three contributions; nonetheless, the sample NaBCN-1Ru only showed a peak located at ~192 eV. The modification con $NaBH_4$ created defects in the structure, reducing the $N_{3\ C}$ creating B=N-C bonds. In the case of NaBCN-1Ru, the presence of B=C-N was inferior to the case of NaBCN, probably due to the reduction of ruthenium to create Ru^0. The B1s peak was deconvoluted in three contributions elemental boron (186.8 eV), B-N (190.3 eV), and B related to oxides or hydroxides (191.9 eV) [49–51]. While the three oxidation states of B are envisaged in the NaBCN sample, when adding the ruthenium precursor to the synthesis, the contribution of BN was not registered.

The optical properties were assessed by the DRS-UV–visible technique. The CN sample displayed radiation absorption in the UV region with a sharp decrease of over 400 nm. The absorption peak around 300–400 nm has been associated in previous works with π–π * transitions in the conjugated ring systems heptazine units [52]. The absorbance of the NaBCN sample was red-shifted improving the absorption in the visible region [13]. The addition of ruthenium enlarged the absorption in the visible region, as depicted in the spectra of Fig. 4**A**. The Kubelka-Munk function is depicted in Fig. 4**B** for the determination of the bandgap energy (see values in Table 1). The bandgap of CN (2.7 eV) was reduced after boron modification in NaBCN (2.6 eV) and further decreased up to 2.0 eV after Ru addition.

Fig. 5 illustrates the local volumetric rate of photon absorption with

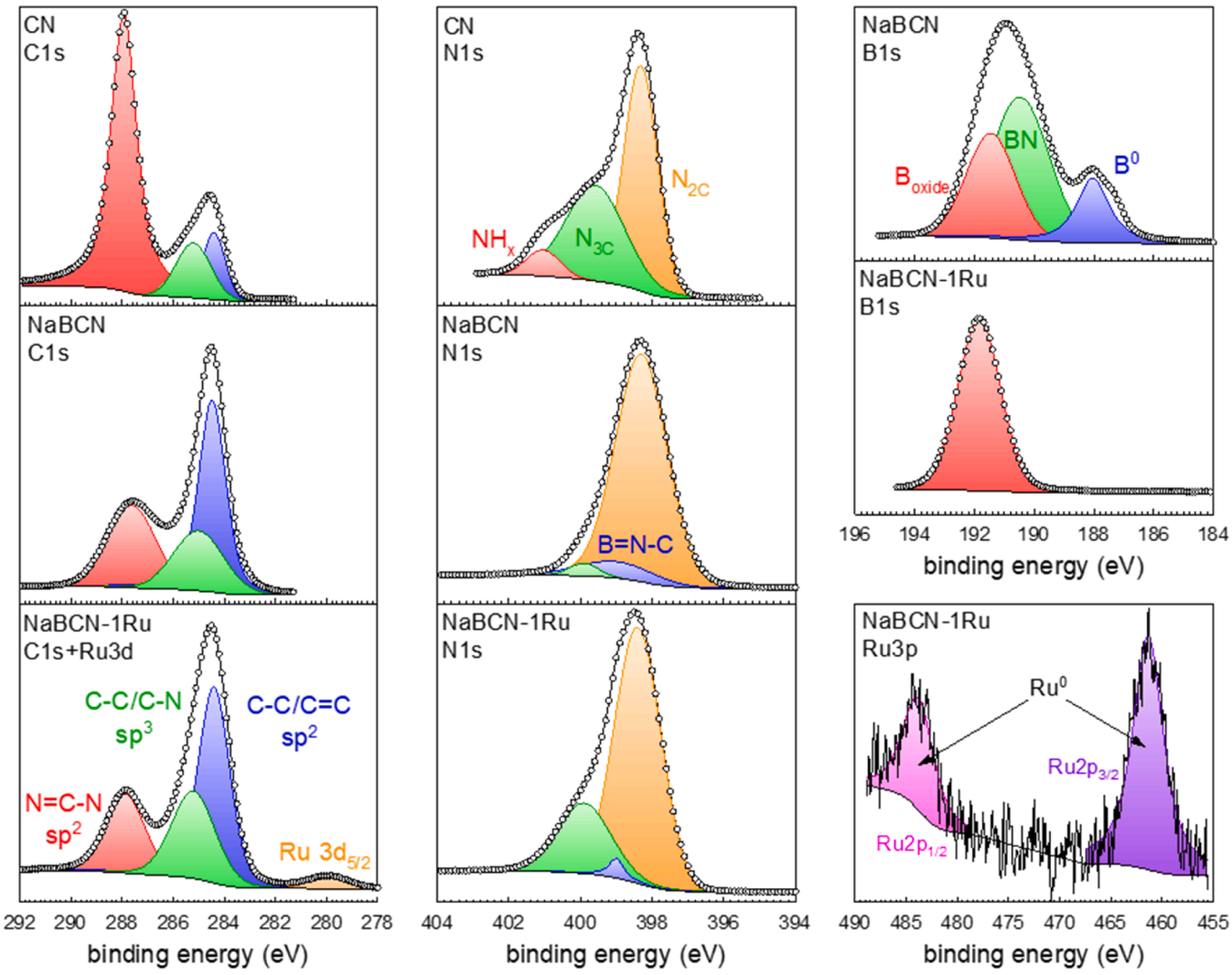

Fig. 3. High-resolution XPS spectra of N1s, C1s, and B1s and Ru3p regions of CN, NaBCN, and NaBCN-4Ru samples.

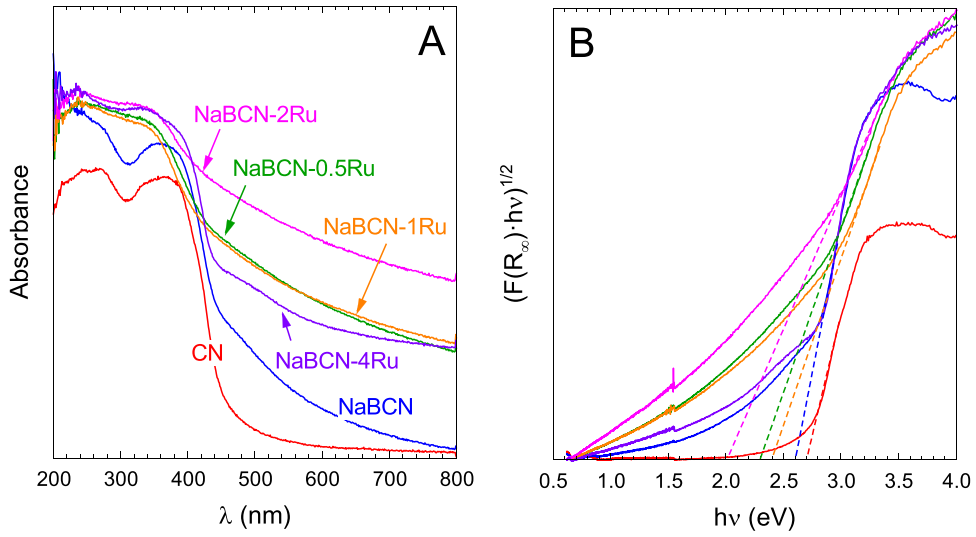

Fig. 4. Absorption DRS-UV–visible spectra (A) and Tauc plot method for the bandgap determination (B) of NaBCN-Ru samples.

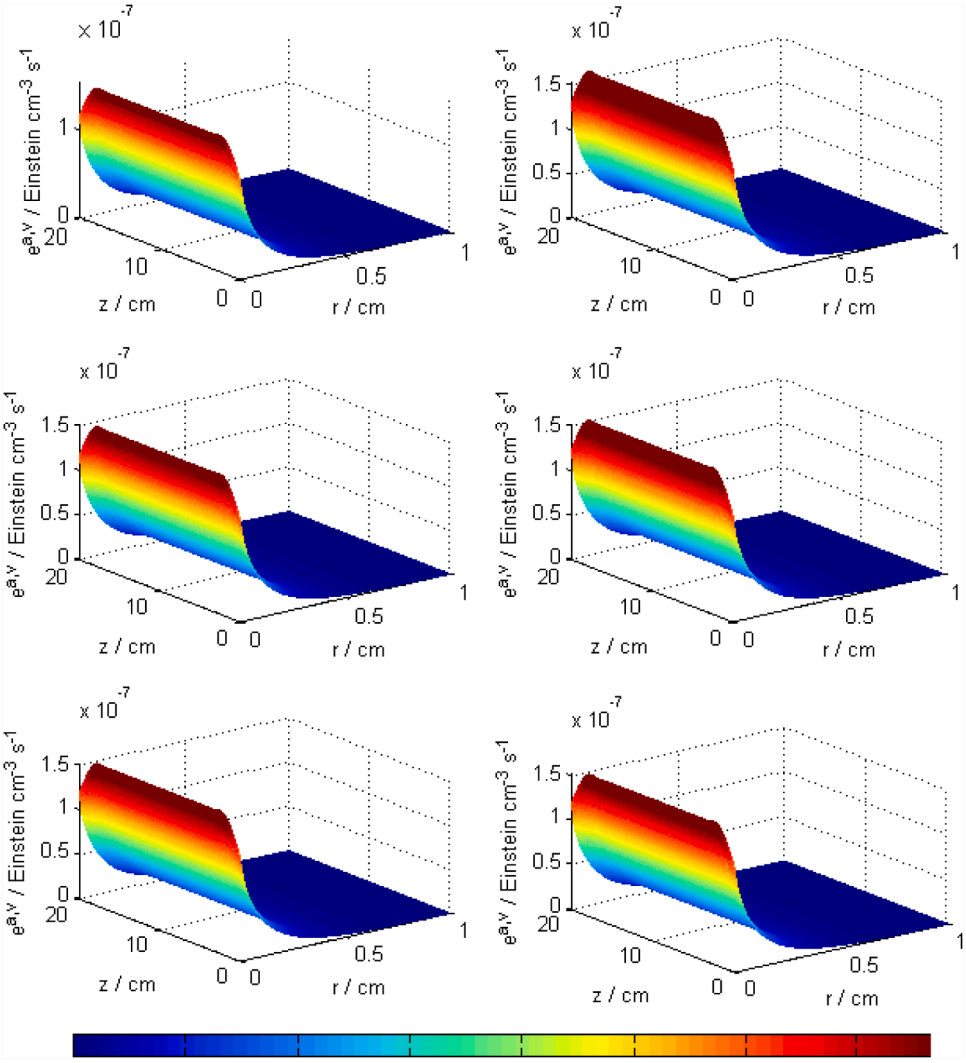

Fig. 5. Local volumetric rate of photon absorption of CN (A), NaBCN (B), and Ru containing samples: (C) NaBCN-0.5Ru, (D) NaBCN-1Ru, (E) NaBCN-2Ru and (F) NaBCN-4Ru.

the radial distance for the different samples. Although optical differences regarding the absorption of radiation were registered in the visible region, at the emitting wavelength of the lamp used, i.e. 365 nm, the differences between the samples were minor. For that reason, the photo absorption rate values (average) and the profiles for each sample are quite similar.

3.2. *Photocatalytic production of benzaldehyde with NaBCN-Ru samples*

The influence of ruthenium presence on the activity of the photocatalysts was assessed in the selective oxidation of benzyl alcohol to benzaldehyde. Fig. 6 depicts the temporal evolution of the remaining concentration of BA and the efficiency of BD production. Also, the observed pseudo-first order rate constant of BA disappearance (k_{BA}) and the average selectivity of BD formation for each catalyst is summarized in Table 2 and Fig. 6.

The CN sample displayed roughly 15% conversion of BA which only was oriented in a 33% BD formation. The modification with $NaBH_4$, i.e. the sample NaBCN, raised the BA conversion to 24% and the selectivity to BD. The deposition of Ru particles onto the NaBCN drastically enhanced the photocatalytic activity, improving the kinetics of BA gradually as the Ru amount increases. As depicted in Fig. 7**A**, the k_{Obs} value was 1.8–6.3-folded depending on the Ru amount incorporated, ranging from 0.5% to 4.0%. The presence of noble metal particles contributes to enhancing the separation of the photogenerated charge as reported in the literature for diverse semiconductors. In this case, Ru acts as an electron sink after the photo-activation of NaBCN, minimizing the undesirable recombination effect. The quantum efficiency shown in Table 2 follows a similar trend to the k_{Obs}, as the photon absorption rate calculated is very similar in each case (see Fig. 5). The presence of Ru enhanced the Q_E value by folding within 3–8 times depending on the Ru load.

An analysis by photoluminescence of the samples provided support to this theory. The emission PL spectrum of CN, see Fig. 7**B**, has a well-defined peak at 455 nm, whose intensity was quite diminished by the modification with $NaBH_4$. The incorporation of boron in the structure has been reported as an effective way to create structural defects that enhance the electronic separation of the photo-generated charges [13,28,48]. Besides, the further Ru deposition eliminated any emitted PL photon, leading to plain PL spectra which suggests an enhanced reduction of the recombination effect due to the improved electrical conductivity and electronic migration of charges [16,17,45]. The photogenerated electrons are expected to migrate from g-C_3N_4 to interfacial Ru due to its affinity to capture electrons acting as a sink which inhibits the recombination effect [45].

Regarding the selectivity, see Fig. 7**A**, the presence of Ru does not exert a positive effect except at a very low concentration, NaBCN-0.5Ru, with a slight improvement if compared to the NaBCN sample, 69.8 vs

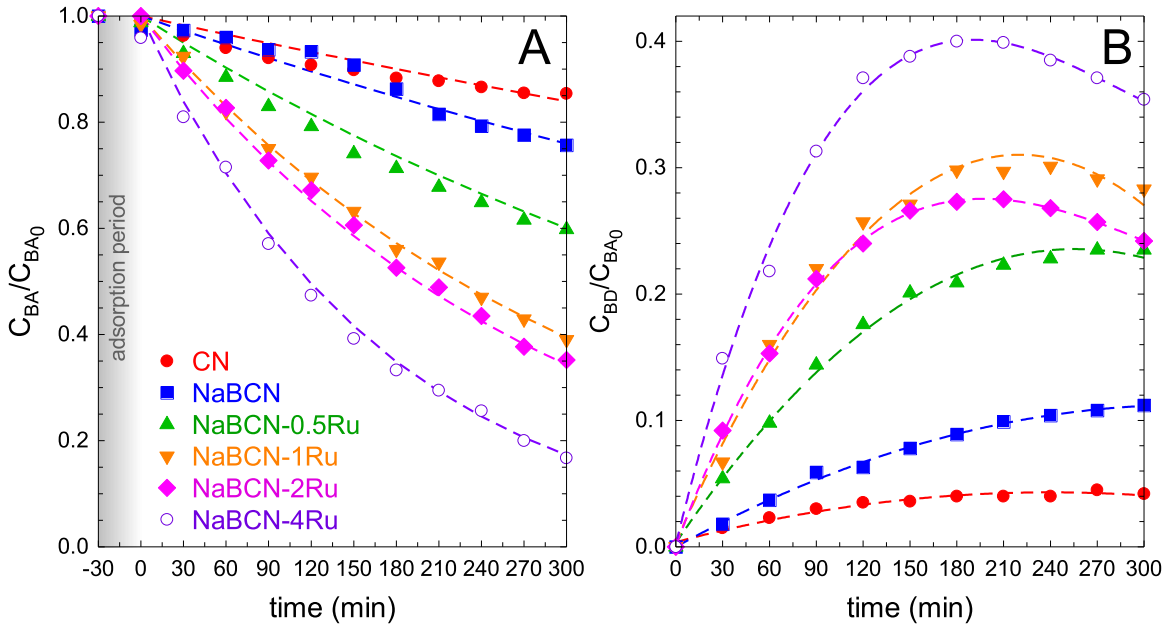

Fig. 6. Photocatalytic production of benzaldehyde with NaBCN-Ru samples at different Ru ratios. Temporal normalized concentration of benzyl alcohol (A) and benzaldehyde (B). *Experimental conditions: V= 350 mL, T = 20°C, $C_{BA,0}$= 0.5 mM; C_{CAT}= 0.5 g L^{-1}; pH= 9.5 ± 0.2.*

Table 2
Kinetic parameters of the photocatalytic production of benzaldehyde with NaBCN-Ru samples.

Sample	$r_{BA,0}\cdot10^3$ (mM min^{-1})	Q_E (%)	k_{BA} (h^{-1})	BA conversion at 3 h (%)	Average BD selectivity (%)
CN	0.243	0.03	0.035	14.6	33.0
NaBCN	0.405	0.04	0.055	24.3	65.5
NaBCN-0.5Ru	0.867	0.09	0.102	40.2	69.8
NaBCN-1Ru	1.267	0.13	0.186	61.0	67.5
NaBCN-2Ru	1.367	0.14	0.214	64.8	62.7
NaBCN-4Ru	2.375	0.24	0.351	83.3	57.3

65.5%. A further raise of Ru decreases the selectivity value. There is, therefore, a confronted effect between selectivity and activity. Considering the results obtained, and the objective of minimization of the noble metal content, 1% of Ru content was selected as the optimum in a compromise of high activity and selectivity. The NaBCN-1Ru sample was selected for further study.

3.3. Photocatalytic mechanism of BA oxidation with NaBCN-1Ru

The relative influence of the different reactive oxidant species (ROS) involved in the photocatalytic activation of NaBCN-1Ru was tentatively by a chemical scavenger study [53]. Fig. 8**A** shows the temporal evolution of BA depletion registered in the blank test and the presence of the selected scavengers, whereas Fig. 8**B** depicts the pseudo-first order rate constant in each case. The impact of superoxide radical ($O_2^{\bullet-}$) was studied by replacing the air bubbling with N_2, with the addition of para-benzoquinone (p-BQ) or tiron. The formation of $O_2^{\bullet-}$ takes place by the reduction of dissolved O_2 adsorbed in the surface of the photocatalyst with the photogenerated electrons. The removal of O_2 by replacement with N_2 led to a 44% decrease in the k_{BA} compared to the blank. The use of p-BQ is widely extended in the scavengers' studies in photocatalytic processes [54], due to the affinity of this substance with $O_2^{\bullet-}$ ($k_{p\text{-}BQ,O2\bullet-}$=1 ×$10^9$ M^{-1} s^{-1} [55]). The addition of p-BQ decreased the k_{BA} considerably, i.e. 81%. Nonetheless, p-BQ can also trap $HO^\bullet$ ($k_{p\text{-}BQ,HO\bullet}$=6.6 ×$10^9$ M^{-1} s^{-1} [56]) and be photolyzed under UVA radiation. It has been reported that the photo-reduction of quinones in aqueous systems yields the formation of $HO^\bullet$ and semiquinone radicals which makes difficult the interpretation of the results [57]. Moreover, the use of p-BQ hides risks due to plausible interactions with the targeted to be converted into substances easily photolyzed [58]. For these reasons, alternative scavengers should be considered before any definitive conclusion. Tiron has been reported as a reliable alternative due to the higher reactivity with superoxide radical, $k_{tiron,O2\bullet-}$= 5 × 10^9 M^{-1} s^{-1} [59], compared to the kinetics of the reaction towards $HO^\bullet$, $k_{tiron,HO\bullet}$= 1.0 × 10^9 M^{-1} s^{-1} [60]. The presence of tiron reduced the k_{BA} to a 36% extent. Taking these results into account, it can be concluded that the oxidation of BA is influenced by $O_2^{\bullet-}$, but not exclusively. The contribution of $HO^\bullet$ was evaluated by the addition of TBA, second-order rate constant $k_{TBA,HO\bullet}$= 6.2 × 10^8 M^{-1} s^{-1} [61]. The effect of TBA was low, with only an 18% of reduction in the k_{BA} for the blank test, so the contribution of $HO^\bullet$ radical can be expected to play a minor role. Finally, the influence of the photogenerated holes was assessed by the presence of oxalic acid [62]. The oxalate anion after being adsorbed onto the surface of the photocatalyst is oxidized by the holes to release CO_2 [41]. Although oxalate anions also can react with $HO^\bullet$, the kinetics is slow $k_{Oxalate,HO\bullet}$= 1.5 × 10^7 M^{-1} s^{-1} [63]. Under the presence of oxalic acid, the k_{BA} was reduced by 64% concerning the blank test, being, therefore, the most relevant species in the process. In summary, the importance of the ROS involved in the process of BA oxidation was: $h^+ > O_2^{\bullet-} > > HO^\bullet$. Other studies involving TiO_2 have identified the importance of holes [64] and superoxide [58] in the process of benzaldehyde production.

Fig. 8B also includes the average selectivity of benzaldehyde production in the presence of the selected scavengers. In the presence of superoxide radical scavengers, i.e. N_2, p-BQ, and tiron, the selectivity was slightly improved if compared to the blank test. The presence of $HO^\bullet$ has been demonstrated to be an unselective route of oxidation [58]. In this sense, the addition of TBA did not affect the selectivity of the process, due to the low impact of $HO^\bullet$ in the process. In the case of the suppression of the holes, the selectivity decreased. This fact provides evidence of the higher selectivity of the holes to the formation of benzaldehyde if compared to the superoxide radical.

Considering the results obtained in the scavengers' studies and data

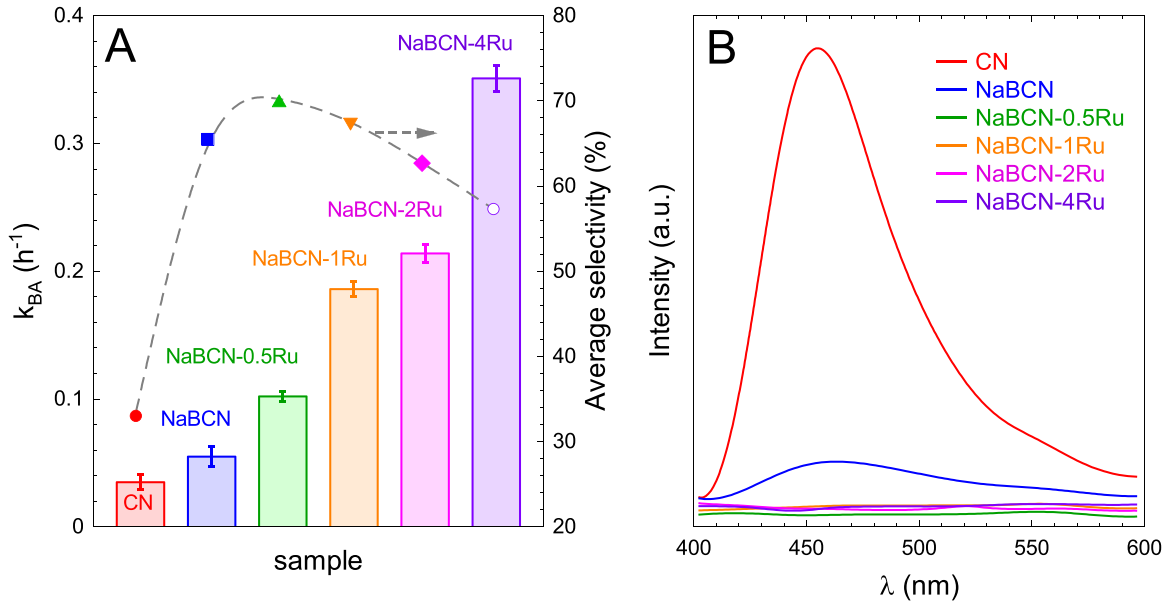

Fig. 7. (A) Pseudo-first order rate constant of BA depletion (k_{BA}) and average selectivity to BD production of NaBCN-Ru samples. (B) PL spectra of the NaBCN-Ru photocatalysts.

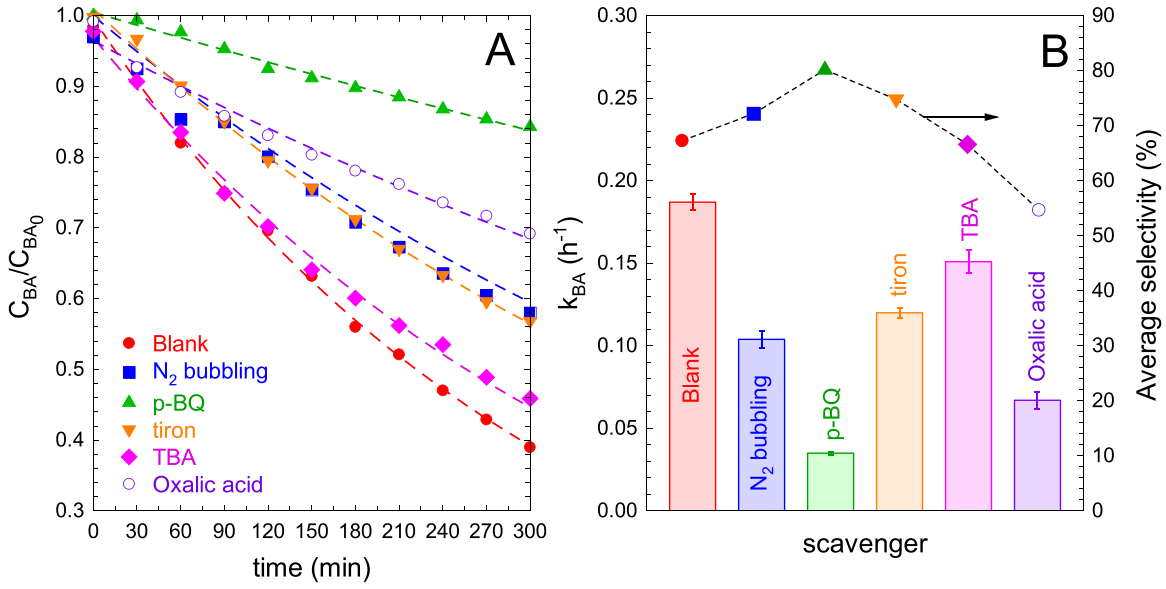

Fig. 8. Photocatalytic production of benzaldehyde with NaBNC-1Ru in the presence of scavengers. Temporal normalized concentration of benzyl alcohol (A), pseudo-first order rate constant of BA depletion, and average BD selectivity (B). *Experimental conditions: V= 350 mL, T = 20°C, $C_{BA,0}$= 0.5 mM; C_{CAT}= 0.5 g L^{-1}; $C_{scavenger}$= 1 mM (p-BQ and tiron) or 10 mM (TBA and oxalic acid); pH= 9.5 ± 0.5.*

obtained by XPS at low energies, a mechanism based on the bands' alignment is proposed (Fig. 9). As aforementioned, modification of CN with B did not display any substantial change in the bandgap value; however, a decrease from 2.6 eV (NaBCN) to 2.3 eV (NaBCN-1Ru) was observed with Ru incorporation. Fig. 9A depicts the XPS spectra at low energies for the evaluation of the minimum valence band energy of NaBCN (1.3 eV) and NaBCN-1Ru (1.9 eV). The obtained energy values are relative to the Fermi level of each material, however, they may suggest a stabilization of the valence band with the deposition of Ru at small proportions on a well-defined CN-B active support. The deposition of Ru is expected to make the photogenerated holes possess higher redox potential (see Fig. 9**B**), supporting the evidence observed in the scavengers' tests, which displayed a higher impact on the oxidation of the alcohol.

4. Conclusions

The modification of the polymeric structure of graphitic carbon nitride results in an efficient strategy to tune the activity of the resulting semiconductor and the selectivity to the oxidation of benzyl alcohol to benzaldehyde in an aqueous solution. This works provides a one-step synthesis route for modification of the g-C_3N_4 structure with boron doping and Ru^0 deposition. The creation of defects on the graphitic structure via B modification enhanced the selectivity towards benzaldehyde due to the improved separation of the photogenerated charges as the photoluminescence response suggested. The deposition of Ru^0 considerably improved the degradation rate of the alcohol since it acts as an electron sink; however, the rise of Ru content rises the conversion unselectively, i.e. decreasing the selectivity of benzaldehyde. A metal

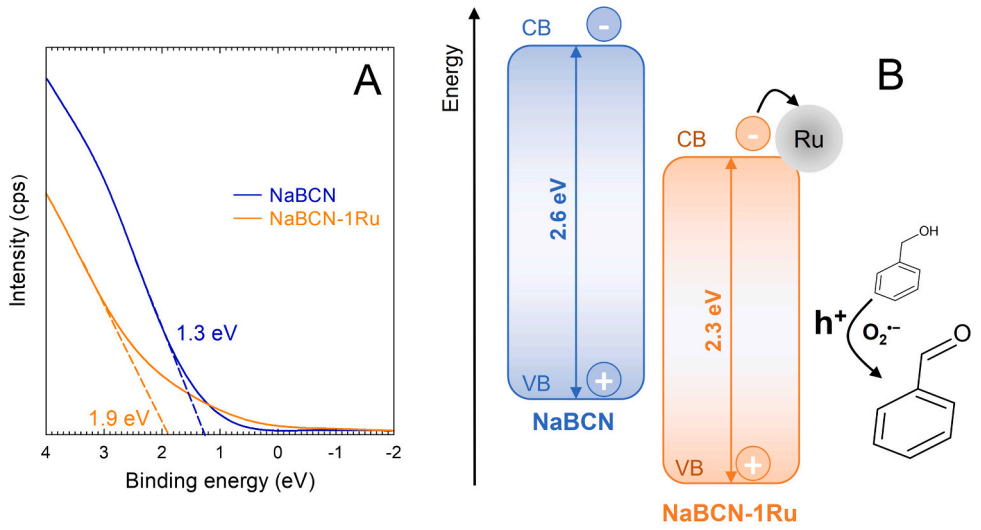

Fig. 9. Determination of the valence band energy by XPS (A) and proposal of the relative band's alignment (B) of NaBCN and NaBCN-1Ru photocatalysts.

proportion of around 1% reached a compromise between both effects. The photo-generated holes followed by the superoxide radical demonstrated to be the main reactive oxidant species involved in the oxidation process. The holes impacted to a higher extent in the selectivity of the process. The estimated valence band energies of the modified graphitic carbon nitride with B and Ru deposition suggest an increase in the redox energy for the valence band with ruthenium deposition, enlarging the oxidative potential of the photo-generated holes.

CRediT authorship contribution statement

Rafael R. Solís: Investigation, Methodology, Formal analysis, Supervision, Writing – original draft, Resources. **M. Alejandra Quintana:** Investigation, Methodology. Gabriel Blázquez: Investigation, Writing – review & editing. F. Mónica Calero: Investigation, Resources, Writing – review & editing. **Mario J. Muñoz-Batista:** Conceptualization, Formal analysis, Supervision, Writing – review & editing, Resources.

Declaration of Competing Interest

The authors declare that they have no known competing financial interests or personal relationships that could have appeared to influence the work reported in this paper.

Data Availability

Data will be made available on request.

Acknowledgements

The authors are grateful to the University of Granada for the "Pre-competitive Research Projects (PPJIA2019-09 and PPJIA2021-34 grants). The authors also thank the help provided by the CIC (Centro de Instrumentación Científica) of the University of Granada. Funding for open access charge: Universidad de Granada / CBUA.

References

[1] J.A.B. Satrio, L.K. Doraiswamy, Production of benzaldehyde: a case study in a possible industrial application of phase-transfer catalysis, Chem. Eng. J. 82 (2001) 43–56, https://doi.org/10.1016/S1385-8947(00)00351-X.
[2] M. Ghahremani, R. Ciriminna, V. Pandarus, A. Scurria, V. La Parola, F. Giordano, G. Avellone, F. Béland, B. Karimi, M. Pagliaro, Green and direct synthesis of benzaldehyde and benzyl benzoate in one pot, ACS Sustain Chem. Eng. 6 (2018) 15441–15446, https://doi.org/10.1021/ACSSUSCHEMENG.8B03893.
[3] A. Akhundi, A. Badiei, G.M. Ziarani, A. Habibi-Yangjeh, M.J. Muñoz-Batista, R. Luque, Graphitic carbon nitride-based photocatalysts: toward efficient organic transformation for value-added chemicals production, Mol. Catal. 488 (2020), 110902, https://doi.org/10.1016/J.MCAT.2020.110902.
[4] S.K. Loeb, P.J.J. Álvarez, J.A. Brame, E.L. Cates, W. Choi, J. Crittenden, D. D. Dionysiou, Q. Li, G. Li-Puma, X. Quan, D.L. Sedlak, T. David Waite, P. Westerhoff, J.H. Kim, The technology horizon for photocatalytic water treatment: sunrise or sunset? Environ. Sci. Technol. 53 (2019) 2937–2947, https://doi.org/10.1021/acs.est.8b05041.
[5] Z. Zhao, Y. Sun, F. Dong, Graphitic carbon nitride based nanocomposites: a review, Nanoscale 7 (2014) 15–37, https://doi.org/10.1039/C4NR03008G.
[6] L. Zhou, H. Zhang, H. Sun, S. Liu, M.O. Tade, S. Wang, W. Jin, Recent advances in non-metal modification of graphitic carbon nitride for photocatalysis: a historic review, Catal. Sci. Technol. 6 (2016) 7002–7023, https://doi.org/10.1039/C6CY01195K.
[7] K. Cerdan, W. Ouyang, J.C. Colmenares, M.J. Muñoz-Batista, R. Luque, A.M. Balu, Facile mechanochemical modification of g-C_3N_4 for selective photo-oxidation of benzyl alcohol, Chem. Eng. Sci. 194 (2019) 78–84, https://doi.org/10.1016/J.CES.2018.04.001.
[8] M.J. Lima, M.J. Sampaio, C.G. Silva, A.M.T. Silva, J.L. Faria, Magnetically recoverable Fe_3O_4/g-C_3N_4 composite for photocatalytic production of benzaldehyde under UV-LED radiation, Catal. Today 328 (2019) 293–299, https://doi.org/10.1016/J.CATTOD.2018.11.018.
[9] Y. Wang, X. Wang, M. Antonietti, Polymeric graphitic carbon nitride as a heterogeneous organocatalyst: from photochemistry to multipurpose catalysis to sustainable chemistry, Angew. Chem. 51 (2012) 68–89, https://doi.org/10.1002/ANIE.201101182.
[10] G. Marcì, E.I. García-López, L. Palmisano, Polymeric carbon nitride (C_3N_4) as heterogeneous photocatalyst for selective oxidation of alcohols to aldehydes, Catal. Today 315 (2018) 126–137, https://doi.org/10.1016/J.CATTOD.2018.03.038.
[11] H. Starukh, P. Praus, Doping of graphitic carbon nitride with non-metal elements and its applications in photocatalysis, Catalysts 10 (2020) 1119, https://doi.org/10.3390/CATAL10101119.
[12] L. Jiang, X. Yuan, Y. Pan, J. Liang, G. Zeng, Z. Wu, H. Wang, Doping of graphitic carbon nitride for photocatalysis: a reveiw, Appl. Catal. B 217 (2017) 388–406, https://doi.org/10.1016/j.apcatb.2017.06.003.
[13] M.A. Quintana, R.R. Solís, M. Ángeles Martín-Lara, G. Blázquez, F. Mónica Calero, M.J. Muñoz-Batista, Enhanced boron modified graphitic carbon nitride for the selective photocatalytic production of benzaldehyde, Sep Purif. Technol. 298 (2022), 121613, https://doi.org/10.1016/J.SEPPUR.2022.121613.
[14] W. Li, X.S. Chu, F. Wang, Y.Y. Dang, X.Y. Liu, X.C. Wang, C.Y. Wang, Enhanced cocatalyst-support interaction and promoted electron transfer of 3D porous g-C_3N_4/GO-M (Au, Pd, Pt) composite catalysts for hydrogen evolution, Appl. Catal. B 288 (2021), 120034, https://doi.org/10.1016/J.APCATB.2021.120034.
[15] Y. Shimoyama, K. Koga, H. Tabe, Y. Yamada, Y. Kon, D. Hong, RuO_2 nanoparticle-embedded graphitic carbon nitride for efficient photocatalytic H_2 evolution, ACS Appl. Nano Mater. 4 (2021) 11700–11708, https://doi.org/10.1021/ACSANM.1C02301.
[16] K. Mori, R. Osaka, K. Naka, D. Tatsumi, H. Yamashita, Ultra-low loading of Ru clusters over graphitic carbon nitride: a drastic enhancement in photocatalytic hydrogen evolution activity, ChemCatChem 11 (2019) 1963–1969, https://doi.org/10.1002/CCTC.201900073.
[17] Z. Yu, Y. Li, A. Torres-Pinto, A.P. LaGrow, V.M. Diaconescu, L. Simonelli, M. J. Sampaio, O. Bondarchuk, I. Amorim, A. Araujo, A.M.T. Silva, C.G. Silva, J. L. Faria, L. Liu, Single-atom Ir and Ru anchored on graphitic carbon nitride for efficient and stable electrocatalytic/photocatalytic hydrogen evolution, Appl. Catal. B 310 (2022), 121318, https://doi.org/10.1016/J.APCATB.2022.121318.

[18] M.J. Lima, P.B. Tavares, A.M.T. Silva, C.G. Silva, J.L. Faria, Selective photocatalytic oxidation of benzyl alcohol to benzaldehyde by using metal-loaded g-C3N4 photocatalysts, Catal. Today 287 (2017) 70–77, https://doi.org/10.1016/J.CATTOD.2016.11.023.

[19] S. Cao, J. Low, J. Yu, M. Jaroniec, Polymeric photocatalysts based on graphitic carbon nitride, Adv. Mater. 27 (2015) 2150–2176, https://doi.org/10.1002/ADMA.201500033.

[20] P. Makuła, M. Pacia, W. Macyk, How to correctly determine the band gap energy of modified semiconductor photocatalysts based on UV–vis spectra, J. Phys. Chem. Lett. 9 (2018) 6814–6817, https://doi.org/10.1021/acs.jpclett.8b02892.

[21] R.R. Solís, M.A. Quintana, M.Á. Martín-Lara, A. Pérez, M. Calero, M.J. Muñoz-Batista, Boosted activity of g-C_3N_4/UiO-66-NH_2 heterostructures for the photocatalytic degradation of contaminants in water, Int J. Mol. Sci. 23 (2022) 12871, https://doi.org/10.3390/IJMS232112871/S1.

[22] J. Lee, J. Kim, W. Choi, Ferrioxalate-polyoxometalate system as a new chemical actinometer, Environ. Sci. Technol. 41 (2007) 5433–5438, https://doi.org/10.1021/ES070474Z.

[23] N. Serpone, Relative photonic efficiencies and quantum yields in heterogeneous photocatalysis, J. Photochem. Photobio. A Chem. 104 (1997) 1–12, https://doi.org/10.1016/S1010-6030(96)04538-8.

[24] G. Li Puma, A. Brucato, Dimensionless analysis of slurry photocatalytic reactors using two-flux and six-flux radiation absorption–scattering models, Catal. Today 122 (2007) 78–90, https://doi.org/10.1016/J.CATTOD.2007.01.027.

[25] O.M. Alfano, D. Bahnemann, A.E. Cassano, R. Dillert, R. Goslich, Photocatalysis in water environments using artificial and solar light, Catal. Today 58 (2000) 199–230, https://doi.org/10.1016/S0920-5861(00)00252-2.

[26] M.J. Muñoz-Batista, A. Kubacka, O. Fontelles-Carceller, D. Tudela, M. Fernández-García, Surface CuO, Bi_2O_3, and CeO_2 species supported in TiO_2-anatase: study of interface effects in toluene photodegradation quantum efficiency, ACS Appl. Mater. Interfaces 8 (2016) 13934–13945, https://doi.org/10.1021/ACSAMI.6B03081.

[27] F. Fina, S.K. Callear, G.M. Carins, J.T.S. Irvine, Structural investigation of graphitic carbon nitride via XRD and neutron diffraction, Chem. Mater. 27 (2015) 2612–2618, https://doi.org/10.1021/ACS.CHEMMATER.5B00411.

[28] X. Wang, B. Liu, X. Xiao, S. Wang, W. Huang, Boron dopant simultaneously achieving nanostructure control and electronic structure tuning of graphitic carbon nitride with enhanced photocatalytic activity, J. Mater. Chem. C. Mater. 9 (2021) 14876–14884, https://doi.org/10.1039/D1TC04142H.

[29] Y. Yan, Q. Yang, Q. Shang, J. Ai, X. Yang, D. Wang, G. Liao, Ru doped graphitic carbon nitride mediated peroxymonosulfate activation for diclofenac degradation via singlet oxygen, Chem. Eng. J. 430 (2022), 133174, https://doi.org/10.1016/J.CEJ.2021.133174.

[30] C. Rajkumar, H. Kim, Interface engineering of ruthenium-supported sulfur-doped graphitic carbon nitride for ultrasensitive electrochemical determination of riboflavin, J. Taiwan Inst. Chem. Eng. 138 (2022), 104470, https://doi.org/10.1016/J.JTICE.2022.104470.

[31] P. Sharma, Y. Sasson, A photoactive catalyst Ru-g-C_3N_4 for hydrogen transfer reaction of aldehydes and ketones, Green. Chem. 19 (2017) 844–852, https://doi.org/10.1039/C6GC02949C.

[32] Z. Ma, S. Zhao, X. Xiong, B. Hu, C. Song, Effect of graphitic carbon nitride on the electronic and catalytic properties of Ru nanoparticles for ammonia synthesis, Catal. Lett. 146 (2016) 2324–2329, https://doi.org/10.1007/s10562-016-1862-y.

[33] S.C. Yan, Z.S. Li, Z.G. Zou, Photodegradation performance of g-C_3N_4 fabricated by directly heating melamine, Langmuir 25 (2009) 10397–10401, https://doi.org/10.1021/LA900923Z.

[34] M.J. Bojdys, J.O. Müller, M. Antonietti, A. Thomas, Ionothermal synthesis of crystalline, condensed, graphitic carbon nitride, Chem. – A Eur. J. 14 (2008) 8177–8182, https://doi.org/10.1002/CHEM.200800190.

[35] D. Zhao, C.-L. Dong, B. Wang, C. Chen, Y.-C. Huang, Z. Diao, S. Li, L. Guo, S. Shen, D. Zhao, B. Wang, Z. Diao, L. Guo, S. Shen, C. Dong, Y. Huang, C. Chen, S. Li, Synergy of dopants and defects in graphitic carbon nitride with exceptionally modulated band structures for efficient photocatalytic oxygen evolution, Adv. Mater. 31 (2019) 1903545, https://doi.org/10.1002/ADMA.201903545.

[36] M. Kim, S. Hwang, J.S. Yu, Novel ordered nanoporous graphitic C_3N_4 as a support for Pt–Ru anode catalyst in direct methanol fuel cell, J. Mater. Chem. 17 (2007) 1656–1659, https://doi.org/10.1039/B702213A.

[37] S. Sunasee, K.H. Leong, K.T. Wong, G. Lee, S. Pichiah, I.W. Nah, B.H. Jeon, Y. Yoon, M. Jang, Sonophotocatalytic degradation of bisphenol A and its intermediates with graphitic carbon nitride, Environ. Sci. Pollut. Res. 26 (2019) 1082–1093, https://doi.org/10.1007/S11356-017-8729-7.

[38] K.S.W. Sing, R.T. Williams, Physisorption hysteresis loops and the characterization of nanoporous materials, Adsorpt. Sci. Technol. 22 (2016) 773–782, https://doi.org/10.1260/0263617053499032.

[39] K.S.W. Sing, D.H. Everett, R.A.W. Haul, L. Moscou, R.A. Pierotti, J. Rouquerol, T. Siemieniewska, Reporting physisorption data for gas/solid systems with special reference to the determination of surface area and porosity, Pure Appl. Chem. 57 (1985) 603–619, https://doi.org/10.1351/PAC198557040603.

[40] M. Thommes, K. Kaneko, A.V. Neimark, J.P. Olivier, F. Rodríguez-Reinoso, J. Rouquerol, K.S.W.W. Sing, Physisorption of gases, with special reference to the evaluation of surface area and pore size distribution (IUPAC Technical Report), Pure Appl. Chem. 87 (2015) 1051–1069.

[41] P. Babu, S. Mohanty, B. Naik, K. Parida, Synergistic effects of boron and sulfur co-doping into graphitic carbon nitride framework for enhanced photocatalytic activity in visible light driven hydrogen generation, Appl. Energy Mater. 1 (2018) 5936–5947, https://doi.org/10.1021/acsaem.8b00956.

[42] H. Cai, D. Han, X. Wang, X. Cheng, J. Liu, L. Jia, Y. Ding, S. Liu, X. Fan, High specific surface area defective g-C_3N_4 nanosheets with enhanced photocatalytic activity prepared by using glyoxylic acid mediated melamine, Mater. Chem. Phys. 256 (2020), 123755, https://doi.org/10.1016/J.MATCHEMPHYS.2020.123755.

[43] Y. Wen, D. Qu, L. An, X. Gao, W. Jiang, D. Wu, D. Yang, Z. Sun, Defective g-C_3N_4 prepared by the $NaBH_4$ reduction for high-performance H_2 production, ACS Sustain. Chem. Eng. 7 (2019) 2343–2349, https://doi.org/10.1021/ACSSUSCHEMENG.8B05124.

[44] D.J. Morgan, Resolving ruthenium: XPS studies of common ruthenium materials, Surf. Interface Anal. 47 (2015) 1072–1079, https://doi.org/10.1002/SIA.5852.

[45] Q. Yang, T. Wang, Z. Zheng, B. Xing, C. Li, B. Li, Constructing interfacial active sites in Ru/g-C_3N_{4-x} photocatalyst for boosting H_2 evolution coupled with selective benzyl-alcohol oxidation, Appl. Catal. B 315 (2022), 121575, https://doi.org/10.1016/J.APCATB.2022.121575.

[46] M. Zhang, J. Chen, H. Li, P. Cai, Y. Li, Z. Wen, Ru-RuO_2/CNT hybrids as high-activity pH-universal electrocatalysts for water splitting within 0.73 V in an asymmetric-electrolyte electrolyzer, Nano Energy 61 (2019) 576–583, https://doi.org/10.1016/J.NANOEN.2019.04.050.

[47] W. Li, Z. Wei, B. Wang, Y. Liu, H. Song, Z. Tang, B. Yang, S. Lu, Carbon quantum dots enhanced the activity for the hydrogen evolution reaction in ruthenium-based electrocatalysts, Mater. Chem. Front 4 (2019) 277–284, https://doi.org/10.1039/C9QM00618D.

[48] H. Xu, Z. Wu, Y. Wang, C. Lin, Enhanced visible-light photocatalytic activity from graphene-like boron nitride anchored on graphitic carbon nitride sheets, J. Mater. Sci. 52 (2017) 9477–9490, https://doi.org/10.1007/S10853-017-1167-6.

[49] U. Caudillo-Flores, D. Rodríguez-Padrón, M.J. Muñoz-Batista, A. Kubacka, R. Luque, M. Fernández-García, Facile synthesis of B/g-C_3N_4 composite materials for the continuous-flow selective photo-production of acetone, Green. Chem. 22 (2020) 4975–4984, https://doi.org/10.1039/D0GC01326A.

[50] M. Dinescu, A. Perrone, A.P. Caricato, L. Mirenghi, C. Gerardi, C. Ghica, L. Frunza, Boron carbon nitride films deposited by sequential pulses laser deposition, Appl. Surf. Sci. 127– 129 (1998) 692–696, https://doi.org/10.1016/S0169-4332(97)00727-7.

[51] M.O. Watanabe, S. Itoh, K. Mizushima, T. Sasaki, Bonding characterization of BC_2N thin films, Appl. Phys. Lett. 68 (1998) 2962, https://doi.org/10.1063/1.116369.

[52] R. You, H. Dou, L. Chen, S. Zheng, Y. Zhang, Graphitic carbon nitride with S and O codoping for enhanced visible light photocatalytic performance, RSC Adv. 7 (2017) 15842–15850, https://doi.org/10.1039/C7RA01036B.

[53] E.M. Rodríguez, G. Márquez, M. Tena, P.M. Álvarez, F.J. Beltrán, Determination of main species involved in the first steps of TiO_2 photocatalytic degradation of organics with the use of scavengers: the case of ofloxacin, Appl. Catal. B 178 (2015) 44–53, https://doi.org/10.1016/j.apcatb.2014.11.002.

[54] M. Pelaez, P. Falaras, V. Likodimos, K. O'Shea, A.A. de la Cruz, P.S.M. Dunlop, J. A. Byrne, D.D. Dionysiou, Use of selected scavengers for the determination of NF-TiO_2 reactive oxygen species during the degradation of microcystin-LR under visible light irradiation, J. Mol. Catal. A Chem. 425 (2016) 183–189, https://doi.org/10.1016/j.molcata.2016.09.035.

[55] B.H.J. Bielski, D.E. Cabelli, R.L. Arudi, A.B. Ross, Reactivity of HO_2/O_2^- radicals in aqueous solution, J. Phys. Chem. Ref. Data 14 (1985) 1041–1100, https://doi.org/10.1063/1.555739.

[56] M. Nien Schuchmann, E. Bothe, J. von Sonntag, C. von Sonntag, Reaction of OH radicals with benzoquinone in aqueous solutions. A pulse radiolysis study, J. Chem. Soc., Perkin Trans. 2 (1998) 791–796, https://doi.org/10.1039/A708772A.

[57] J.T. Schneider, D.S. Firak, R.R. Ribeiro, P. Peralta-Zamora, Use of scavenger agents in heterogeneous photocatalysis: truths, half-truths, and misinterpretations, Phys. Chem. Chem. Phys. 22 (2020) 15723–15733, https://doi.org/10.1039/d0cp02411b.

[58] D.A. Giannakoudakis, A. Qayyum, M. Barczak, R.F. Colmenares-Quintero, P. Borowski, K. Triantafyllidis, J.C. Colmenares, Mechanistic and kinetic studies of benzyl alcohol photocatalytic oxidation by nanostructured titanium (hydro)oxides: do we know the entire story? Appl. Catal. B 320 (2023), 121939 https://doi.org/10.1016/J.APCATB.2022.121939.

[59] C.L. Greenstock, R.W. Miller, The oxidation of tiron by superoxide anion. Kinetics of the reaction in aqueous solution and in chloroplasts, Biochim. Biophys. Acta 396 (1975) 11–16, https://doi.org/10.1016/0005-2728(75)90184-X.

[60] W. Bors, M. Saran, C. Michel, Pulse-radiolytic investigations of catechols and catecholamines II. Reactions of Tiron with oxygen radical species, BBA - Gen. Subj. 582 (1979) 537–542, https://doi.org/10.1016/0304-4165(79)90145-4.

[61] M.S. Alam, B.S.M. Rao, E. Janata, ·OH reactions with aliphatic alcohols: Evaluation of kinetics by direct optical absorption measurement. A pulse radiolysis study, Radiat. Phys. Chem. 67 (2003) 723–728, https://doi.org/10.1016/S0969-806X(03)00310-4.

[62] B.R. Shah, U.D. Patel, Mechanistic aspects of photocatalytic degradation of Lindane by TiO_2 in the presence of Oxalic acid and EDTA as hole-scavengers, J. Environ. Chem. Eng. 9 (2021), 105458, https://doi.org/10.1016/J.JECE.2021.105458.

[63] B.G. Ershov, E. Janata, M.S. Alam, A.V. Gordeev, A pulse radiolysis study of the reactions of the hydrated electron and hydroxyl radical with the oxalate ion in neutral aqueous solution, High. Energy Chem. 42 (2008) 1–6, https://doi.org/10.1134/s0018143908010013.

[64] L. Zhao, B. Zhang, X. Xiao, F.L. Gu, R.Q. Zhang, Roles of the active species involved in the photocatalytic oxidation of benzyl alcohol into benzaldehyde on TiO_2 under UV light: experimental and DFT studies, J. Mol. Catal. A Chem. 420 (2016) 82–87, https://doi.org/10.1016/J.MOLCATA.2016.03.012.